Author Manuscript

Author Manuscript

Author Manuscript

Author Manuscript

HHS Public Access

Author manuscript

J Immunol. Author manuscript; available in PMC 2018 February 09.

Published in final edited form as:

J Immunol. 2016 December 15; 197(12): 4838–4847. doi:10.4049/jimmunol.1600692.

Generation of Immunity against Pathogens via Single-Domain Antibody–Antigen Constructs

Joao N. Duarte, **Juan J. Cragnolini**, **Lee Kim Swee**, **Angelina M. Bilate**, **Justin Bader**, **Jessica R. Ingram**, **Ali Rashidfarrokhi**, **Tao Fang**, **Ariën Schiepers**, **Leo Hanke**, and **Hidde L. Ploegh**

Whitehead Institute, Department of Biology, Massachusetts Institute of Technology, Cambridge, MA 02142

Abstract

mAbs specific for surface proteins on APCs can serve as Ag-delivery vehicles that enhance immunogenicity. The practical use of such constructs is limited by the challenge of expressing and modifying full-sized mAbs. We generated single-domain Ab fragments (VHHs) specific for class II MHC (MHCII), CD11b, and CD36. VHH sequences were modified by inclusion of a C-terminal sortase motif to allow site-specific conjugation with various Ag payloads. We tested T cell activation using VHHs that target distinct APC populations; anti-MHCII adducts elicited strong activation of $CD4^+$ T cells, whereas anti-CD11b showed $CD8^+$ T cell activation superior to targeting via MHCII and CD36. Differences in Ag presentation among constructs were unrelated to dendritic cell subtype or routing to acidic compartments. When coupled to antigenic payloads, anti-MHCII VHH primed Ab responses against GFP, ubiquitin, an OVA peptide, and the α-helix of influenza hemagglutinin's stem; the last afforded protection against influenza infection. The versatility of the VHH scaffold and sortase-mediated covalent attachment of Ags suggests their broader application to generate desirable immune responses.

Targeted delivery of Ags to professional APCs enhances immune responses (1–4). Covalent fusions of an anti-DEC205 mAb with an antigenic payload of interest were used for induction of CD4 and CD8 T cell responses (1, 4). Other surface proteins expressed on dendritic cells (DCs) have been exploited for similar purposes (5). However, the underlying cell biological mechanisms responsible for the efficient induction of immune responses by these means remain to be explored more fully.

Full-sized Abs can be used as fusion partners for antigenic payloads of interest, but low expression yields and structural complexity hamper the generation of such constructs. The same holds true for single-chain variable fragments derived from mAbs; these require careful design of the requisite linker to obtain stable single-chain variable fragments in

Address correspondence and reprint requests to Dr. Hidde L. Ploegh, Whitehead Institute, Department of Biology, Massachusetts Institute of Technology, 9 Cambridge Center, Cambridge, MA 02142. ploegh@wi.mit.edu.
ORCIDs: 0000-0002-0430-5165 (J.B.); 0000-0002-5185-364X (A.S.); 0000-0001-5514-2418 (L.H.); 0000-0002-1090-6071 (H.L.P.).

The online version of this article contains supplemental material.

Disclosures

The authors have no financial conflicts of interest.

Author Manuscript Author Manuscript Author Manuscript Author Manuscript

adequate yield. As an alternative to this approach, we undertook the production of a smaller and simpler delivery vehicle in the form of single-domain Ab fragments (VHHs) composed of the V region of the H chain–only Abs present in camelids. VHHs, also known as single-domain Abs or nanobodies, can be expressed recombinantly in bacteria to yield proteins that retain full Ag-binding properties and lack the Fc portion of full-sized mAbs (6). Compared with classical Abs, VHHs have several advantages, including smaller size, ease of expression, monomeric behavior, and thermostability (6, 7). VHHs identified by phage display and expressed recombinantly in bacteria do not require glycosylation or disulfide bonding for Ag recognition. By reducing the size of the Ag-delivery vehicle, we also expect to improve tissue penetration.

We generated anti–class II MHC (MHCII), anti-CD11b, and anti-CD36 VHHs and analyzed their suitability as vehicles for the induction of immune responses in distinct DC populations. MHCII products, integrins (CD11b), and scavenger receptors (CD36) are abundantly expressed on APCs. Their molecular and cell biological properties are sufficiently different to warrant their exploration as possible targets for Ag delivery. The comparatively short $t_{1/2}$ of VHHs in the circulation has not stood in the way of highly efficient targeting of lymphoid organs via an MHCII-specific VHH, as shown by noninvasive imaging using positron emission tomography (8). We installed a sortase-recognition site on each VHH to facilitate site-specific conjugation to Ag payloads using a modified transpeptidase, sortase A, from *Staphylococcus aureus* (9). The sortase-catalyzed reaction results in the installation of the substituent of interest offered as an oligo-glycine–based nucleophile (Fig. 1A). Their ease of expression in bacteria and the flexibility of the sortase platform to enable installation of structurally diverse Ags make Ag-modified VHHs an appealing strategy to enhance immune responses.

Materials and Methods

Construction of VHH library and expression of recombinant VHHs

An adult alpaca was immunized with intact unfractionated mouse splenocytes (5×10^6 cells per injection) at 2–3-wk intervals for a total of seven injections. We assessed the host response by immunoblotting of alpaca serum against membrane and cytosolic fractions of murine splenocytes that were isolated by selective plasma membrane permeabilization. Mononuclear cells from peripheral blood were isolated from the immunized alpaca by Ficoll gradient separation, followed by an established VHH library–generation protocol (10). Total RNA was extracted (RNeasy RNA Purification kit; QIAGEN), and cDNA was prepared (Superscript III First Strand Synthesis Kit; Life Technologies). The diversity of the cDNA preparation was maximized by using three sets of complementary oligonucleotides for first-strand cDNA synthesis: oligo-dT, random hexamers, and Ig-specific primers. The DNA sequences of the signal sequence from conventional and H chain–only Ig genes are not distinguishable based on the use of specific primers. However, two unique and distinct hinge regions (short and long hinge) are generated between the VHH domain and the C region (CH2). Thus, we amplified the VHH repertoire from the immune animal using alpaca VHH specific–primers that target these particular hinge sequences. The purified VHH PCR products were pooled and ligated into a phagemid vector to construct a phage display library

Author Manuscript Author Manuscript Author Manuscript Author Manuscript

through in-frame fusion of the amplified VHH sequences with the pIII gene of the M13 phagemid. The diversity of the phagemid library was estimated by serial dilution. The resulting VHH library consisted of ~10^8 independent clones. We performed several rounds of panning against mouse splenocytes, as well as DC and B cell lines. VHH clones that showed reactivity by ELISA were enriched and expressed in WK6 *Escherichia coli* and grown in Terrific Broth overnight at 30°C after isopropyl β-D-thiogalactopyranoside induction (1 mM) at an OD_{600} of 0.6. VHHs were harvested from the periplasm by osmotic shock and purified by metal ion affinity using Ni-NTA agarose beads (QIAGEN) size-exclusion chromatography (SEC) on a Superdex 75 16/600 (GE Healthcare) in PBS or Tris HCl (50 mM [pH 7.5]).

VHH selection and immunoprecipitation assays

Expressed VHHs were sortagged to G_3–Alexa Fluor 647 and buffer exchanged using PD-10 columns (GE Healthcare). To identify VHHs that recognize surface molecules on APCs, Alexa Fluor–labeled VHHs were used to costain C57BL/6 wild-type splenocytes with commercial mAbs (M5/114.15.2 anti-MHCII, eBio1D3 anti-CD19, HL3 anti-CD11c, M1/70 anti-CD11b, HM36 anti-CD36, and BM8 anti-F4/80), and they were analyzed by FACS (BD Fortessa). Cell surface molecules recognized by the selected VHHs were identified by immunoprecipitation. A20 cells were lysed with NET buffer (50 mM Tris, 0.5% Nonidet P-40, 150 mM NaCl, 5 mM EDTA [pH 7.4]) and incubated with sortagged biotinylated VHH7 for 1 h at 4°C. Cell lysates were incubated with Streptavidin beads (MyOne Dynabeads; Invitrogen) for 1 h at 4°C. MutuDCs (11) were incubated with biotinylated DC13 or DC20 VHHs for 0 or 5 min at 37°C. Cells were then lysed with NET buffer and incubated with FG beads (Tamagawa). After three rounds of washing, immunoprecipitates were analyzed by SDS-PAGE and silver stained.

Sortase reactions

All sortase reactions were performed in 50 mM Tris (pH 7.5), 150 mM NaCl, and 10 mM $CaCl_2$ and incubated for 90 min at 15–20°C. The reagent concentrations were 100 μM VHH, 1–3 μM anti-DEC205, 500 μM nucleophile, and 2.5 μM 5M-sortase (9). Residual uncoupled substrate and sortase were removed by adsorption to Ni-NTA beads (QIAGEN). Identity of the final product, purified by gel filtration, was confirmed by SDS-PAGE and liquid chromatography–mass spectrometry (LC-MS) (Supplemental Fig. 1). All peptides used as nucleophiles were synthesized at the MIT Biopolymers & Proteomics Core Facility. $(Gly)_5$-GFP and $(Gly)_5$-ubiquitin were expressed in BL21(DE3) *E. coli* and grown in Terrific Broth overnight at 30°C after isopropyl β-D-thiogalactopyranoside induction (1 mM) at an OD_{600} of 0.6. Proteins were extracted using a French press and purified by metal ion affinity using Ni-NTA agarose beads (QIAGEN) SEC on a Superdex 75 16/600 (GE Healthcare) in PBS or Tris HCl (50 mM [pH 7.5]) and NaCl (150 mM). All VHH–nucleophile constructs were purified by SEC in endotoxin-free conditions.

VHH7 characterization

The binding capacity of VHH7 was compared with that of two conventional fluorescent-labeled anti-MHCII mAbs: M5 (I-$A^{b,d,q}$; I-$E^{d,k}$) and AF6 (I-A^b). The mean fluorescence intensities were obtained by staining mouse splenocytes at 4°C with increasing

Author Manuscript Author Manuscript Author Manuscript Author Manuscript

concentrations of VHH7–Alexa Fluor 647, M5–Alexa Fluor 647, or AF6–Alexa Fluor 647. GraphPad Prism was used for curve fitting and to calculate the K_a, K_d, and K_D. The affinity range is based on the observed experimental error (SE). The binding capacity of VHH7 to recombinant MHCII-CLIP variants was measured by surface plasmon resonance. K_D was determined on a Biacore T100 using a Streptavidin Sensor Chip (BR100032; GE Healthcare), purified VHH7 biotinylated in a sortase A–catalyzed reaction, and different allotypic versions of fully assembled class II products in complex with class II–associated invariant chain peptide as the analyte. K_a and K_d of VHH7 were calculated for I-A^b, I-A^d, I-A^u, I-A^k, and I-A^{g7} and were used to determine K_D. Experimental binding data were adjusted using full concentrations with local R_{max}.

Mice

C57BL/6, BALB/c, μMT, Baft3-deficient, MHCII-deficient, CD11b-deficient, and CD36-deficient mice were purchased from the Jackson Laboratory, and OT-I and OT-II Rag-deficient mice were purchased from Taconic Technologies.

In vitro experiments

Splenic DCs were collected from 5–8-wk-old C57BL/6 mice and purified with CD11c or *Pan*-DC MACS MicroBeads (Miltenyi Biotec). Splenic DCs were activated with 1 μg/ml of anti-CD40 (1645-01; South-ernBiotech) and 12.5 μg/ml of polyinosinic-polycytidylic acid [poly(I:C)] (P0913; Sigma-Aldrich) for 1 h in RPMI 1640 (Life Technologies) supplemented with heat-inactivated fetal calf serum (IFS), washed, and incubated with VHH constructs for 45 min at different concentrations. DCs were incubated with different concentrations of chloroquine from 1 h prior to and up to 4 h after application of VHHs. After purification, all VHH constructs showed endotoxin levels < 1 EU (88282 Thermo Scientific Pierce LAL Chromogenic Endotoxin Quantitation Kit). Cells were washed and incubated with CSFE-labeled OT-I or OT-II $Rag^{-/-}$ T cells from transgenic mice for 18–36 h. T cells were labeled with 2 μM CFSE (Sigma-Aldrich). CD69 expression on T cells was measured 18 h after coculture, and CSFE levels of the transferred T cells were measured by FACS after 36 h of coculture to assess proliferation.

Imaging

For intracellular VHH staining, splenic DCs were incubated with 1–2 μg of Alexa Fluor 647–labeled VHHs on ice for 30 min, washed, plated at 37°C for different times with 10 nM LysoTracker (Life Technologies), and incubated with anti-CD45–Alexa Fluor 488 Ab on ice (30F11; BioLegend). Cells were fixed with 4% PFA for 15 min, washed, put in solution with PBS and glycerol, imaged with a Zeiss RPI Spinning Disk microscope, and analyzed by Fiji/ImageJ.

In vivo experiments

Single-cell suspensions from spleen and lymph nodes were obtained from CD45.2 OT-I/$Rag^{-/-}$ or OT-II/$Rag^{-/-}$ transgenic mice. Cells (1×10^6) were labeled with CFSE and adoptively transferred i.v. into congenitally marked CD45.1 hosts (C57BL/6, 6–10 wk old) or derivative strains. Between 6 and 24 h after cell transfer, mice were immunized i.p. with VHH7 (0.2

Author Manuscript Author Manuscript Author Manuscript Author Manuscript

μg), anti-DEC205 (1 μg), or control substrate fused to OT-II or OT-I peptide in the presence of 50 μg of poly(I:C) (P0913; Sigma-Aldrich) and 25 μg of anti-CD40 (1645-01; SouthernBiotech) in the injected solution. At days 3–7 after immunization, CD8 or CD4 T cell proliferation was measured by CFSE dilution as analyzed by flow cytometry.

BALB/c mice were left untreated or were immunized i.p. at weeks 1, 3, and 5 with equimolar amounts of VHH7 fused to payload (20–30 μg), payload alone, payload in solution with VHH7, or nucleophile fused to a control VHH. All immunizations were conducted with 25 μg of anti-CD40 and 50 μg of poly(I:C). Sera were collected at week 6 postimmunization, and Ab production was analyzed by immunoblot and ELISA.

For influenza infection, mice were anesthetized and inoculated by in-tranasal administration of 1.25×10^5 EID_{50} of purified influenza virus A H3N2/X-31 (Charles River Laboratories) in 40 μl of PBS. Body weight and survival (persistent weight loss > 25% of initial body weight) were assessed daily for 12 d postinoculation.

Immunoblotting

Mouse sera were used for immunoblotting against various concentrations of GFP, ubiquitin, OVA, or recombinant H3N2 hemagglutinin (HA) (A/Aichi/ 2/1968; Sino Biological). Sera were used at 1:500–3000 dilutions, and secondary Abs were used at a 1:10,000 dilution (anti-mouse IgG-HRP NXA931 [GE Healthcare], anti-His–HRP 1014992 [QIAGEN], anti-H3N2 HA 11056-MM03-50 [Sino Biological]). Quantification of densitometric traces of immunoblotted sera from immunized mice was performed with ImageJ.

ELISA

Plates were coated with 5 μg of H3N2/X-31 recombinant HA (Sino Biological). Sera from mice immunized with VHH7 dimer-$HA2_{12–63}$ were added as serial dilutions in 0.5% IFS PBS-T for 1 h at room temperature. Plates were washed and incubated with anti-IgG1–HRP (SouthernBiotech), anti-IgG2a–HRP (SouthernBiotech), or anti-IgG2b–HRP (SouthernBiotech) at a 1:4000 dilution in 0.5% IFS PBS-T for 1 h. Plates were developed with OptEIATMB (BD), the reaction was stopped with 1 M sulfuric acid, and the plate was read at 450 nm absorbance.

Results

Bioengineering and characterization of VHHs

We constructed a phage display library of VHHs from an alpaca immunized with mouse splenocytes, starting with PBLs from the immunized animal, and performed several rounds of panning against mouse splenocytes, as well as against DC and B cell lines. We selected phage clones based on DNA sequences enriched for phage that were recovered on each of the target cell populations. Selected VHHs were subcloned into a bacterial expression vector, such that the resultant VHH contained the LPETG sequence as a C-terminal sortase motif, followed by a $(His)_6$-tag to facilitate purification. The presence of the sortase motif allows coupling of any payload that carries a $(Gly)_3$ extension at the N terminus (Fig. 1A). VHHs were expressed in the bacterial periplasm and purified using standard methods.

Author Manuscript Author Manuscript Author Manuscript Author Manuscript

We selected three VHHs from the VHH library that target, but are not limited to, distinct DC populations: VHH7, which recognizes mouse MHCII products (Fig. 2) on all DC subsets; DC13, which recognizes CD11b on $CD8^-$ DCs; and DC20, specific for CD36 on $CD8^+$ DCs (Fig. 1B, 1C) (12, 13). The targets of the individual VHHs were identified by immunoprecipitation using cell lysates prepared from DC (11) and B cell lymphoma cell lines as source material, which was followed by SDS-PAGE, silver staining, and liquid chromatography–tandem mass spectrometry of the immunoprecipitated products (Fig. 1D). To confirm the liquid chromatography–tandem mass spectrometry results, we conjugated the respective VHHs to Alexa Fluor 647 using sortase and costained splenocytes from wild-type and the corresponding knockout mice with a conventional fluorescently labeled mAb counterpart of similar specificity (Fig. 1E). The combined results established the specificity of each of the VHHs as anti-MHCII (VHH7), anti-CD11b, (DC13) and anti-CD36 (DC20).

Receptor-mediated T cell activation is independent of the DC subtype targeted

mAbs, and in particular anti-DEC205, have been used extensively to modulate immune responses (1, 14, 15). Genetic or chemical fusions of antigenic payloads with mAbs yield formulations that can elicit CD4 and CD8 T cell responses (5, 14). To test the ability of VHH7-, DC13-, and DC20-based covalent adducts to activate T cells, we used sortase to attach OT-I or OT-II peptides, the immunodominant epitopes from OVA recognized by CD8 and CD4 TCR-transgenic mice, respectively. Splenic DCs were incubated in vitro with each adduct, followed by incubation with CFSE-labeled OT-I or OT-II $Rag^{-/-}$ T cells for 36 h to assess T cell proliferation. OT-I/II peptides and an anti-GFP VHH (16) (Enh) were used as positive and negative controls, respectively. Although VHH7-OTI failed to induce proliferation of OT-I CD8 T cells in vitro, VHH7-OTII induced strong proliferation of OT-II CD4 T cells. This proliferation was more pronounced than that elicited by the DC13 (anti-CD11b) and DC20 (anti-CD36) adducts. However, targeting of CD11b via DC13 showed the strongest CD8 T cell activation, despite its preferred binding specificity for $CD8^-$ DCs (Fig. 3A, 3B). Because CD11b targeting showed improved cross-presentation of Ags compared with MHCII, we used fluorescently labeled VHH7 or DC13 to track the internalization of VHH–receptor complexes and acidic subcellular compartments. Despite the fact that DC13 was internalized and degraded faster than VHH7, they displayed similar rates of colocalization to acidic vesicles, as identified by LysoTracker staining. Although VHH7 reaches lysosomes later than DC13, it seems to persist longer in these compartments (Fig. 3C, 3D). To test whether a reduction in pH within lysosomes, as well as an increase in lysosomal membrane permeabilization, could enhance cross-presentation of Ags delivered by VHH7, we incubated splenic DCs with increasing concentrations of chloroquine (17, 18). Upon stimulation with 2 ng of VHH-OTI conjugates, VHH7 exhibited an expansion of OT-I T cell proliferation comparable to DC13 (Fig. 3E). However, cells treated with bafilomycin A1, to raise lysosomal pH without increasing lysosomal membrane permeabilization, did not show the same effect (data not shown), suggesting that the confinement of VHH7 in acidic compartments hinders cross-presentation of the attached Ag.

VHH7 targets $CD8^-$ DCs to activate $CD4^+$ T cells

The VHH7-OTII adduct induces CD4 T cell proliferation in vitro. We used the same VHH7-OTII adduct to compare its capacity for Ag delivery in vitro and in vivo with that of the anti-

Author Manuscript Author Manuscript Author Manuscript Author Manuscript

DEC205–OTII conjugate (14). We produced VHH7-OTII, anti-DEC205–OTII, and GFP-OTII conjugates to test activation of OT-II CD4 T cells by splenic DCs. After 18 h, T cell activation was monitored by increased surface expression of CD69. On a molar basis, VHH7-OTII was more efficient at activating $CD4^+$ T cells than were anti-DEC205–OTII and anti-GFP–OTII (Fig. 4A, 4B). We confirmed this result in vivo with CD45.1 mice that received allotypically marked CFSE-labeled CD45.2 OT-II $Rag^{-/-}$ T cells and that were immunized i.p. with equivalent amounts of VHH7-OTII, anti-DEC205–OTII, or GFP-OTII in combination with anti-CD40 and poly(I:C) as the adjuvant (Fig. 4C). Enhanced CD4 T cell activation by VHH7 adducts is dependent on coadministration of adjuvant; mice not immunized with adjuvant showed limited CD4 T cell activation, whereas the response was measurably stronger when adjuvants were included (Fig. 4D, 4E). The same protocol was used to compare the proliferation of transferred OT-I CD8 T cells in mice immunized with VHH7-OTI, anti-DEC205–OTI, or anti-GFP–OTI conjugates in vivo. As seen in vitro, VHH7-OTI failed to activate OT-I T cells in vivo (Fig. 4F). To identify the APCs responsible for CD4 T cell activation upon VHH7-OTII administration, we compared the proliferation of $CD4^+$ T cells in C57BL/6 wild-type, μMT (B cell–deficient), $Baft3^{-/-}$ ($CD8^+$ DC-deficient), and $MHCII^{-/-}$ mice. CFSE-labeled OT-II $Rag^{-/-}$ T cells were transferred i.v., followed by i.p. injection of VHH7-OTII or Enh-OTII in combination with anti-CD40 and poly(I:C). Because μMT and $Baft3^{-/-}$ mice showed results that were similar to wild-type mice, we inferred that VHH7-OTII activation of $CD4^+$ T cells is primarily dependent on $CD8^-$ DCs (Fig. 4G, 4H).

Generation of B cell immunity against protein and peptide Ags by VHH7 delivery

Given the ability of VHH7 adducts to trigger a robust CD4 T cell response, we examined the possibility of priming Ab responses against payloads attached covalently to VHH7. As proof-of-principle, we tested the construct's ability to trigger an immune response against GFP. For comparison, we used free Ag (GFP) or a mixture of VHH7 and free Ag at the same concentrations used for the covalent adducts. After primary immunization and two successive boosts, coadministered with poly(I:C) and anti-CD40, the presence of serum Abs was assessed in an immunoblot against GFP. Neither free GFP nor a mixture of GFP and VHH7 elicited a strong Ab response, whereas the covalent adduct did (Fig. 5A). Quantitation of the immunoblots suggested an ~100-fold enhancement in Ab titers (Fig. 5B). Thus, increased Ab titers are readily attainable through administration of the covalently modified VHH.

We chose additional Ag models to further confirm the usefulness of VHH7 as a platform for priming robust Ab responses. We used yeast ubiquitin (96% identical to mouse) as a poorly immunogenic small protein and OVA's OBI-17mer peptide (19), a dominant OVA B cell epitope. For the covalent VHH7–Ag conjugates tested, we observed markedly improved Ab responses. Neither the mixture of ubiquitin or OBI and VHH7, nor of Ag conjugated to a control VHH, elicited an Ab response under conditions in which the covalent conjugates were efficacious (Fig. 5C, 5D).

Author Manuscript Author Manuscript Author Manuscript Author Manuscript

Dimerization of VHH7 enhances B cell immunity

Using the same expression and purification protocols, we created a genetic homodimer of VHH7 equipped with a C-terminal sortase motif (Fig. 6A, 6B) and fused it enzymatically to Alexa Fluor 647. Mice injected i.v. with fluorescent versions of VHH7 homodimer showed an ~6-fold increase in splenocyte staining by cytofluorimetry compared with the VHH7 monomer. Fluorescence of the VHH7 dimer was detectable for up to 24 h after injection (Fig. 6C). Stained splenocytes also showed greater fluorescence intensity by microscopy (Fig. 6D, 6E). To explore whether an increase in avidity and half-life further improved Ab responses, we conjugated VHH7 dimer to OT-II and OBI peptide. Despite similar proliferation of OT-II T cells primed with monomer and dimer constructs at different concentrations (Fig. 6F), quantification of immunoblots probed with sera suggested an ~2-fold increase in Ab titers against OVA of mice immunized with VHH7-OBI dimer relative to the monomeric form (Fig. 6G, 6H).

In vivo protection against influenza infection

We extended this immunization protocol to a sequence of influenza's H3N2 HA2 α-helix ($HA2_{12–63}$) in which conserved epitopes were identified that are the target of broadly neutralizing Abs (20–23). Sera from mice immunized with the VHH7 dimer fused to the HA2 α-helix showed a strong IgG1 response against H3N2/X-31 recombinant HA by ELISA and immunoblot (Fig. 7A, 7B). To test whether this humoral response could provide immunity to influenza, we tested serum neutralization of H3N2/X-31 in vitro and challenged mice with an intranasal inoculate of the same strain (Fig. 7C). Despite a lack of virus neutralization in vitro (data not shown), the administration of $HA2_{12–63}$ covalently attached to VHH7 dimer improved survival and conferred protection against influenza infection.

Discussion

We investigated whether targeting broadly distinct APC populations using single-domain Abs (VHHs) could be used as an Ag-delivery platform to trigger immune responses. We explored Ab responses against Ags that might otherwise be poorly immunogenic. We demonstrate that VHH7, DC13, and DC20 recognize mouse MHCII, CD11b, and CD36, respectively, and that a sortase-catalyzed reaction is an efficient means of fusing Ags to VHHs in a site-specific fashion. We show that anti-MHCII (VHH7) adducts activate $CD8^-$ DCs to elicit stronger CD4 T cell proliferation than anti-CD11b (DC13), anti-CD36 (DC20), and anti-DEC205 (14), whereas the DC13 adduct shows improved CD8 T cell proliferation. Mice immunized with VHH7 enzymatically fused to GFP, yeast ubiquitin, the OBI-17mer peptide, or the α-helix of influenza's HA stem all elicited potent humoral responses compared with the Ag delivered in solution and simply mixed with VHH7. Ab responses were enhanced an additional ~2-fold by a dimeric version of VHH7. Mice immunized with VHH7-H3N2 $HA2_{12–63}$ showed improved protection against influenza H3N2/X-31 infection. The purpose of these experiments was not so much to identify the actual DC subsets targeted but to compare the efficacy of VHH fusions that target nonoverlapping sets of APCs based on the published expression patterns of these markers. It should be emphasized that none of the molecules targeted are expressed exclusively on DCs and that, in vivo, other $MHCII^+$, $CD36^+$, or $CD11b^+$ cells may contribute as well.

Author Manuscript Author Manuscript Author Manuscript Author Manuscript

Abs display high selectivity and affinity and have been the preferred platform for Ag targeting. Despite the development of Ag-delivery systems that enable T cell activation, targeting approaches that enhance Ab responses need improvement (24). Pioneering work done almost three decades ago on B cell responses evoked by targeting of APCs via MHCII products showed enhanced Ab titers against avidin when administered as a non-covalent adduct with chemically biotinylated anti-MHCII mAbs (2). Other studies showed high levels of Ab responses against antigenic payloads elicited by targeting of Clec9A, CD11c, and CD180 with mAb or Fab fragments conjugated to OVA and injected into naive mice (25–27). The efficiency of these responses largely correlates with the pattern of expression of these receptors on APCs (25, 26). In the cases cited, the production of the relevant immunogens used chemical conjugation to purified mAbs, a method that is rarely site specific unless mAbs are engineered specifically for that purpose [e.g., by the introduction of a free and exposed Cys residue (28) or by making use of modifications, such as aldehyde tags (29)].

VHHs have been used extensively as neutralizing Abs (6) in the manner of conventional Abs. In this article, we show that VHHs, when equipped with a sortase motif, can be used to deliver proteins or peptides to APCs to generate humoral immunity. The use of site-specific chemical fusions can overcome many of the drawbacks of the genetic conjugation of Ags or of rather unspecific and often unpredictable chemical-modification strategies, such as maleimide- or succinimide-mediated cross-linking (30). Conventional conjugation methods and classical Abs or their derivatives are also less suited to large-scale manufacturing and high-throughput approaches (30). Sortase-catalyzed ligations have the advantage of simplicity and great flexibility in terms of the type of molecule that can be attached, whether is to a full-sized mAb (14) or an Ab fragment (8, 31). Genetic modifications of proteins by the addition of an N-terminal $(Gly)_n$ extension (with or without the use of a protease cleavage site) or the synthesis of peptides with N-terminal Gly extensions is straightforward and imposes few limits on the type of soluble Ag that can be used for ligation.

The VHH7-GFP fusion elicited an ~100-fold increase in Ab titers, as measured by immunoblotting, compared with GFP administered alone or compared with a simple mixture of Ag with VHH7. We extended this approach to yeast ubiquitin (96% identical to mouse; 3 aa difference); OBI, an immunodominant B cell epitope (19); and the α-helical stem region of influenza HA, an accessible part of the stem where conserved epitopes that elicit broadly neutralizing Abs have been identified (20–23). A strong B cell response was recorded even when using a poorly immunogenic small protein like yeast ubiquitin or when reducing the size of the payload attached to VHH7 from a protein to a peptide, as for OBI or the HA2 α-helix. The striking difference in titers elicited by covalent VHH7-peptide fusions and the in vivo protective effect of VHH7-HA2 α-helix immunization suggest the possibility of using VHH7 to enhance immunogenicity of B cell epitopes carried by other viral, bacterial, or fungal pathogens. VHHs, by virtue of their ease of production and modification, as well as their ability to transcend the barriers imposed by genetic fusions (31), position these small Ab fragments as promising tools to (re)engineer immune responses.

We used a similar approach to deliver OT-I and OT-II epitopes in vitro to APCs. Previous studies indicated a superior ability of $CD8^+$ DCs to activate cytotoxic T cells (32–34). In

Author Manuscript Author Manuscript Author Manuscript Author Manuscript

these $CD8^+$ DCs, an intracellular environment that curtails Ag degradation and facilitates Ag transfer from endocytic compartments to the cytosol for cross-presentation may contribute to this property (35, 36). Despite the fact that the intracellular environment in $CD8^+$ DCs is conducive to Ag cross-presentation, the efficacy of receptor-mediated Ag presentation seems to depend on other factors, such as the identity of the receptor(s) involved (37–39). In our model, the DC subset targeted, rates of receptor internalization, and routing of Ags to acidic compartments do not seem to be major determinants of the efficiency of Ag presentation. Other studies (15, 40) also suggested that the function of DC subtypes and other APCs, such as B cells (41) and macrophages (42), may overlap in their ability to initiate a CD8 T cell response. Their intrinsic characteristics and propensity to cross-present may be overshadowed by the type of surface receptor targeted. CD11b and CD36 represent molecularly quite distinct types of receptors that are expressed on $CD8^-$ and $CD8^+$ DCs, respectively. Both are internalized in the course of phagocytosis (43). Targeting of CD11b via DC13 showed stronger proliferation of $CD8^+$ T cells than did targeting via CD36, suggesting that, regardless of the proteolytic activity present in lysosomes, Ag presentation can still be efficient. A greater difference in $CD8^+$ T cell proliferation was observed between CD11b and MHCII, despite the fact that both receptors are routed to acidic compartments in DCs. These differences may result, in part, from predominant targeting of $MHCII^{high}$ DCs by VHH7, because mature DCs acidify their endocytic compartments more efficiently (44, 45).

Supplementary Material

Refer to Web version on PubMed Central for supplementary material.

Acknowledgments

This work was supported by National Institutes of Health Pioneer Award DP1-GM106409-03 and National Institutes of Health Grants R01-AI087879-06 and R01-GM100518-04 (all to H.L.P.). J.N.D. is a Calouste Gulbenkian scholar, funded by the Calouste Gulbenkian Foundation, the Champalimaud Foundation, the Portuguese Science and Technology Foundation, and the Portuguese Ministry of Health.

We thank Eric Spooner (Proteomic Core Facility, Whitehead Institute) for mass spectrometry analysis and the MIT Biopolymers and Proteomics Core Facility for peptide synthesis.

Abbreviations used in this article

DC	dendritic cell
HA	hemagglutinin
IFS	heat-inactivated fetal calf serum
LC-MS	liquid chromatography–mass spectrometry
MHCII	class II MHC
poly(I:C)	polyinosinic-polycytidylic acid
SEC	size-exclusion chromatography

Author Manuscript Author Manuscript Author Manuscript Author Manuscript

VHH single-domain Ab fragment

References

1. Bonifaz LC, Bonnyay DP, Charalambous A, Darguste DI, Fujii S, Soares H, Brimnes MK, Moltedo B, Moran TM, Steinman RM. In vivo targeting of antigens to maturing dendritic cells via the DEC-205 receptor improves T cell vaccination. J Exp Med. 2004; 199:815–824. [PubMed: 15024047]
2. Carayanniotis G, Barber BH. Adjuvant-free IgG responses induced with antigen coupled to antibodies against class II MHC. Nature. 1987; 327:59–61. [PubMed: 3472080]
3. Kawamura H, Berzofsky JA. Enhancement of antigenic potency in vitro and immunogenicity in vivo by coupling the antigen to anti-immunoglobulin. J Immunol. 1986; 136:58–65. [PubMed: 3079611]
4. Hawiger D, Inaba K, Dorsett Y, Guo M, Mahnke K, Rivera M, Ravetch JV, Steinman RM, Nussenzweig MC. Dendritic cells induce peripheral T cell unresponsiveness under steady state conditions in vivo. J Exp Med. 2001; 194:769–779. [PubMed: 11560993]
5. Cohn L, Delamarre L. Dendritic cell-targeted vaccines. Front Immunol. 2014; 5:255. [PubMed: 24910635]
6. Muyldermans S. Nanobodies: natural single-domain antibodies. Annu Rev Biochem. 2013; 82:775–797. [PubMed: 23495938]
7. Helma J, Cardoso MC, Muyldermans S, Leonhardt H. Nanobodies and recombinant binders in cell biology. J Cell Biol. 2015; 209:633–644. [PubMed: 26056137]
8. Rashidian M, Keliher EJ, Bilate AM, Duarte JN, Wojtkiewicz GR, Jacobsen JT, Cragnolini J, Swee LK, Victora GD, Weissleder R, Ploegh HL. Noninvasive imaging of immune responses. Proc Natl Acad Sci USA. 2015; 112:6146–6151. [PubMed: 25902531]
9. Guimaraes CP, Witte MD, Theile CS, Bozkurt G, Kundrat L, Blom AE, Ploegh HL. Site-specific C-terminal and internal loop labeling of proteins using sortase-mediated reactions. Nat Protoc. 2013; 8:1787–1799. [PubMed: 23989673]
10. Maass DR, Sepulveda J, Pernthaner A, Shoemaker CB. Alpaca (*Lama pacos*) as a convenient source of recombinant camelid heavy chain antibodies (VHHs). J Immunol Methods. 2007; 324:13–25. [PubMed: 17568607]
11. Fuertes Marraco SA, Grosjean F, Duval A, Rosa M, Lavanchy C, Ashok D, Haller S, Otten LA, Steiner QG, Descombes P, et al. Novel murine dendritic cell lines: a powerful auxiliary tool for dendritic cell research. Front Immunol. 2012; 3:331. [PubMed: 23162549]
12. Hashimoto D, Miller J, Merad M. Dendritic cell and macrophage heterogeneity in vivo. Immunity. 2011; 35:323–335. [PubMed: 21943488]
13. Shay T, Kang J. Immunological Genome Project and systems immunology. Trends Immunol. 2013; 34:602–609. [PubMed: 23631936]
14. Swee LK, Guimaraes CP, Sehrawat S, Spooner E, Barrasa MI, Ploegh HL. Sortase-mediated modification of αDEC205 affords optimization of antigen presentation and immunization against a set of viral epitopes. Proc Natl Acad Sci USA. 2013; 110:1428–1433. [PubMed: 23297227]
15. Chatterjee B, Smed-Sörensen A, Cohn L, Chalouni C, Vandlen R, Lee BC, Widger J, Keler T, Delamarre L, Mellman I. Internalization and endosomal degradation of receptor-bound antigens regulate the efficiency of cross presentation by human dendritic cells. Blood. 2012; 120:2011–2020. [PubMed: 22791285]
16. Kirchhofer A, Helma J, Schmidthals K, Frauer C, Cui S, Karcher A, Pellis M, Muyldermans S, Casas-Delucchi CS, Cardoso MC, et al. Modulation of protein properties in living cells using nanobodies. Nat Struct Mol Biol. 2010; 17:133–138. [PubMed: 20010839]
17. Accapezzato D, Visco V, Francavilla V, Molette C, Donato T, Paroli M, Mondelli MU, Doria M, Torrisi MR, Barnaba V. Chloroquine enhances human CD8+ T cell responses against soluble antigens in vivo. J Exp Med. 2005; 202:817–828. [PubMed: 16157687]
18. Boya P, Gonzalez-Polo RA, Poncet D, Andreau K, Vieira HL, Roumier T, Perfettini JL, Kroemer G. Mitochondrial membrane permeabilization is a critical step of lysosome-initiated apoptosis induced by hydroxychloroquine. Oncogene. 2003; 22:3927–3936. [PubMed: 12813466]

Author Manuscript Author Manuscript Author Manuscript Author Manuscript

19. Avalos AM, Bilate AM, Witte MD, Tai AK, He J, Frushicheva MP, Thill PD, Meyer-Wentrup F, Theile CS, Chakraborty AK, et al. Monovalent engagement of the BCR activates ovalbumin-specific transnuclear B cells. J Exp Med. 2014; 211:365–379. [PubMed: 24493799]
20. Corti D, Voss J, Gamblin SJ, Codoni G, Macagno A, Jarrossay D, Vachieri SG, Pinna D, Minola A, Vanzetta F, et al. A neutralizing antibody selected from plasma cells that binds to group 1 and group 2 influenza A hemagglutinins. Science. 2011; 333:850–856. [PubMed: 21798894]
21. Ekiert DC, Bhabha G, Elsliger MA, Friesen RH, Jongeneelen M, Throsby M, Goudsmit J, Wilson IA. Antibody recognition of a highly conserved influenza virus epitope. Science. 2009; 324:246–251. [PubMed: 19251591]
22. Ekiert DC, Friesen RH, Bhabha G, Kwaks T, Jongeneelen M, Yu W, Ophorst C, Cox F, Korse HJ, Brandenburg B, et al. A highly conserved neutralizing epitope on group 2 influenza A viruses. Science. 2011; 333:843–850. [PubMed: 21737702]
23. Okuno Y, Isegawa Y, Sasao F, Ueda S. A common neutralizing epitope conserved between the hemagglutinins of influenza A virus H1 and H2 strains. J Virol. 1993; 67:2552–2558. [PubMed: 7682624]
24. Xu W, Banchereau J. The antigen presenting cells instruct plasma cell differentiation. Front Immunol. 2014; 4:504. [PubMed: 24432021]
25. Chaplin JW, Chappell CP, Clark EA. Targeting antigens to CD180 rapidly induces antigen-specific IgG, affinity maturation, and immunological memory. J Exp Med. 2013; 210:2135–2146. [PubMed: 24019553]
26. Lahoud MH, Ahmet F, Kitsoulis S, Wan SS, Vremec D, Lee CN, Phipson B, Shi W, Smyth GK, Lew AM, et al. Targeting antigen to mouse dendritic cells via Clec9A induces potent CD4 T cell responses biased toward a follicular helper phenotype. J Immunol. 2011; 187:842–850. [PubMed: 21677141]
27. White AL, Tutt AL, James S, Wilkinson KA, Castro FV, Dixon SV, Hitchcock J, Khan M, Al-Shamkhani A, Cunningham AF, Glennie MJ. Ligation of CD11c during vaccination promotes germinal centre induction and robust humoral responses without adjuvant. Immunology. 2010; 131:141–151. [PubMed: 20465572]
28. Junutula JR, Raab H, Clark S, Bhakta S, Leipold DD, Weir S, Chen Y, Simpson M, Tsai SP, Dennis MS, et al. Site-specific conjugation of a cytotoxic drug to an antibody improves the therapeutic index. Nat Biotechnol. 2008; 26:925–932. [PubMed: 18641636]
29. Carrico IS, Carlson BL, Bertozzi CR. Introducing genetically encoded aldehydes into proteins. Nat Chem Biol. 2007; 3:321–322. [PubMed: 17450134]
30. Popp MW, Antos JM, Grotenbreg GM, Spooner E, Ploegh HL. Sortagging: a versatile method for protein labeling. Nat Chem Biol. 2007; 3:707–708. [PubMed: 17891153]
31. Witte MD, Cragnolini JJ, Dougan SK, Yoder NC, Popp MW, Ploegh HL. Preparation of unnatural N-to-N and C-to-C protein fusions. Proc Natl Acad Sci USA. 2012; 109:11993–11998. [PubMed: 22778432]
32. Dudziak D, Kamphorst AO, Heidkamp GF, Buchholz VR, Trumpfheller C, Yamazaki S, Cheong C, Liu K, Lee HW, Park CG, et al. Differential antigen processing by dendritic cell subsets in vivo. Science. 2007; 315:107–111. [PubMed: 17204652]
33. Hildner K, Edelson BT, Purtha WE, Diamond M, Matsushita H, Kohyama M, Calderon B, Schraml BU, Unanue ER, Diamond MS, et al. Batf3 deficiency reveals a critical role for CD8alpha+ dendritic cells in cytotoxic T cell immunity. Science. 2008; 322:1097–1100. [PubMed: 19008445]
34. Schnorrer P, Behrens GM, Wilson NS, Pooley JL, Smith CM, El-Sukkari D, Davey G, Kupresanin F, Li M, Maraskovsky E, et al. The dominant role of CD8+ dendritic cells in cross-presentation is not dictated by antigen capture. Proc Natl Acad Sci USA. 2006; 103:10729–10734. [PubMed: 16807294]
35. Delamarre L, Pack M, Chang H, Mellman I, Trombetta ES. Differential lysosomal proteolysis in antigen-presenting cells determines antigen fate. Science. 2005; 307:1630–1634. [PubMed: 15761154]
36. Savina A, Peres A, Cebrian I, Carmo N, Moita C, Hacohen N, Moita LF, Amigorena S. The small GTPase Rac2 controls phagosomal alkalinization and antigen crosspresentation selectively in CD8(+) dendritic cells. Immunity. 2009; 30:544–555. [PubMed: 19328020]

Author Manuscript Author Manuscript Author Manuscript Author Manuscript

37. Dadaglio G, Fayolle C, Zhang X, Ryffel B, Oberkampf M, Felix T, Hervas-Stubbs S, Osicka R, Sebo P, Ladant D, Leclerc C. Antigen targeting to CD11b+ dendritic cells in association with TLR4/TRIF signaling promotes strong CD8+ T cell responses. J Immunol. 2014; 193:1787–1798. [PubMed: 25024388]

38. Kamphorst AO, Guermonprez P, Dudziak D, Nussenzweig MC. Route of antigen uptake differentially impacts presentation by dendritic cells and activated monocytes. J Immunol. 2010; 185:3426–3435. [PubMed: 20729332]

39. Segura E, Durand M, Amigorena S. Similar antigen cross-presentation capacity and phagocytic functions in all freshly isolated human lymphoid organ-resident dendritic cells. J Exp Med. 2013; 210:1035–1047. [PubMed: 23569327]

40. Cohn L, Chatterjee B, Esselborn F, Smed-Sörensen A, Nakamura N, Chalouni C, Lee BC, Vandlen R, Keler T, Lauer P, et al. Antigen delivery to early endosomes eliminates the superiority of human blood BDCA3+ dendritic cells at cross presentation. J Exp Med. 2013; 210:1049–1063. [PubMed: 23569326]

41. Heit A, Huster KM, Schmitz F, Schiemann M, Busch DH, Wagner H. CpG-DNA aided cross-priming by cross-presenting B cells. J Immunol. 2004; 172:1501–1507. [PubMed: 14734727]

42. Bernhard CA, Ried C, Kochanek S, Brocker T. CD169+ macrophages are sufficient for priming of CTLs with specificities left out by cross-priming dendritic cells. Proc Natl Acad Sci USA. 2015; 112:5461–5466. [PubMed: 25922518]

43. Flannagan RS, Jaumouillé V, Grinstein S. The cell biology of phagocytosis. Annu Rev Pathol. 2012; 7:61–98. [PubMed: 21910624]

44. Sepulveda FE, Maschalidi S, Colisson R, Heslop L, Ghirelli C, Sakka E, Lennon-Duménil AM, Amigorena S, Cabanie L, Manoury B. Critical role for asparagine endopeptidase in endocytic Toll-like receptor signaling in dendritic cells. Immunity. 2009; 31:737–748. [PubMed: 19879164]

45. Trombetta ES, Ebersold M, Garrett W, Pypaert M, Mellman I. Activation of lysosomal function during dendritic cell maturation. Science. 2003; 299:1400–1403. [PubMed: 12610307]

Author Manuscript Author Manuscript Author Manuscript Author Manuscript

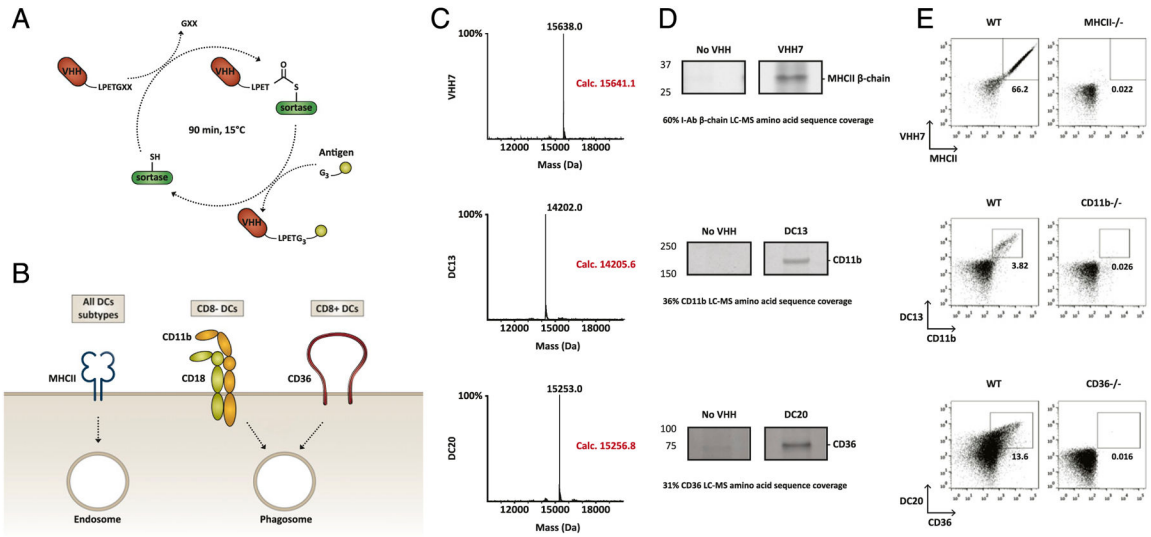

FIGURE 1.

Site-specific fusion of antigenic payloads to single-domain Abs for receptor-mediated Ag delivery. (**A**) Schematic diagram of a camelid H chain–only Ab and its derived variable domain fragment (15 kDa). VHH sequences were cloned with a periplasmic expression sequence that allows bacterial extraction by osmotic shock and a sortase recognition motif for site-specific conjugation of antigenic payloads for in vivo targeting. The sortase reaction is complete after 90 min at 15°C. The enzymatic reaction is followed by a two-step purification for enzyme and nucleophile removal. (**B**) Schematic representation of the surface molecules targeted by VHHs generated from an alpaca immunized with intact mouse splenocytes: MHCII (VHH7); CD11b (DC13), and CD36 (DC20). (**C**) LC-MS of VHH adducts after Ni-NTA purification and SEC. (**D**) Recognition of VHH cell surface targets by immunoprecipitation. A20 and MutuDCs were incubated or not with biotinylated VHH for different times. Cell lysates were then incubated with streptavidin or neutravidin beads, washed, and analyzed by SDS-PAGE for silver staining. (**E**) VHH recognition of cell surface molecules by flow cytometry. Costaining of splenocytes from wild-type and corresponding knockout mice with a conventional fluorescently labeled mAb counterpart of similar specificity. Each figure is representative of two or three independent experiments.

Author Manuscript Author Manuscript Author Manuscript Author Manuscript

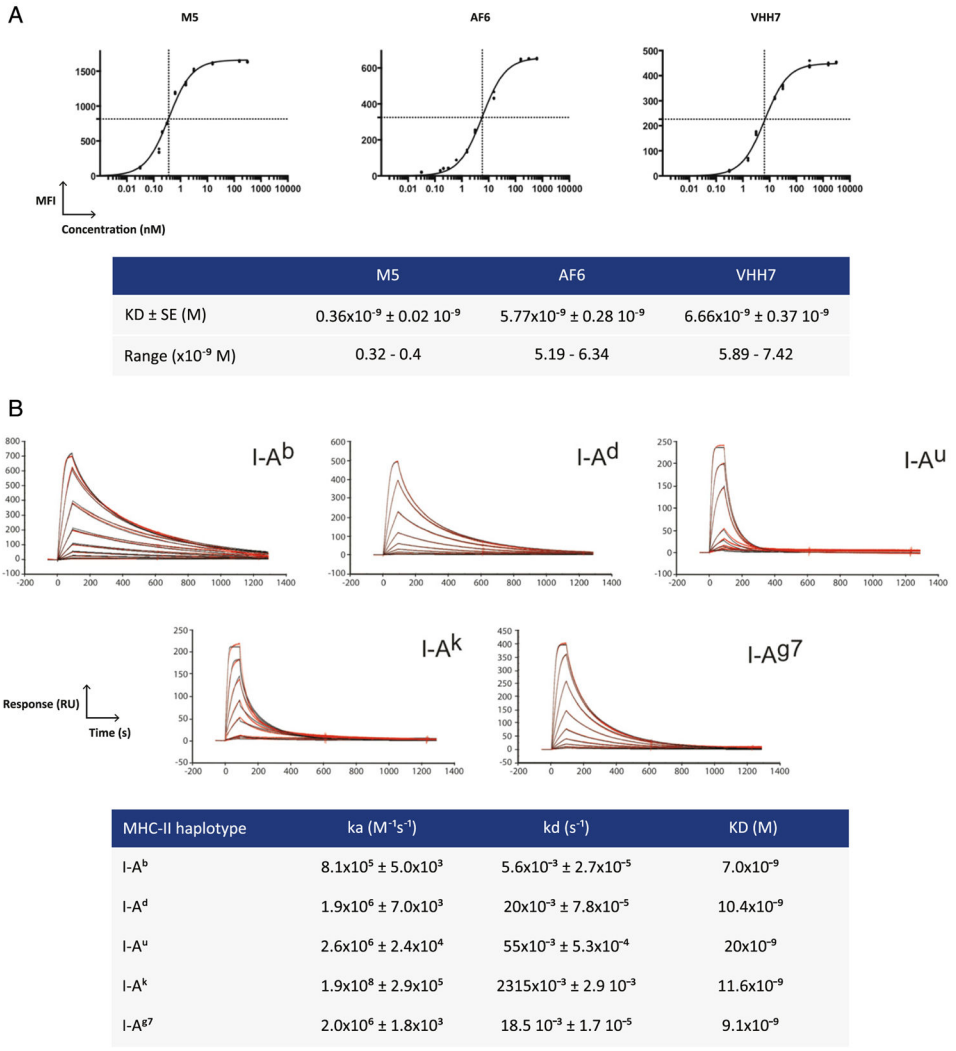

	M5	AF6	VHH7
KD ± SE (M)	$0.36x10^{-9} \pm 0.02\ 10^{-9}$	$5.77x10^{-9} \pm 0.28\ 10^{-9}$	$6.66x10^{-9} \pm 0.37\ 10^{-9}$
Range ($x10^{-9}$ M)	0.32 - 0.4	5.19 - 6.34	5.89 - 7.42

MHC-II haplotype	ka ($M^{-1}s^{-1}$)	kd (s^{-1})	KD (M)
I-A^b	$8.1x10^5 \pm 5.0x10^3$	$5.6x10^{-3} \pm 2.7x10^{-5}$	$7.0x10^{-9}$
I-A^d	$1.9x10^6 \pm 7.0x10^3$	$20x10^{-3} \pm 7.8x10^{-5}$	$10.4x10^{-9}$
I-A^u	$2.6x10^6 \pm 2.4x10^4$	$55x10^{-3} \pm 5.3x10^{-4}$	$20x10^{-9}$
I-A^k	$1.9x10^8 \pm 2.9x10^5$	$2315x10^{-3} \pm 2.9\ 10^{-3}$	$11.6x10^{-9}$
I-A^{g7}	$2.0x10^6 \pm 1.8x10^3$	$18.5\ 10^{-3} \pm 1.7\ 10^{-5}$	$9.1x10^{-9}$

FIGURE 2.

VHH7 affinity and recognition of polymorphic MHCII variants. (**A**) Comparison of the binding capacity of VHH7–Alexa Fluor 647 with that of two conventional fluorescent-labeled anti-MHCII mAbs [M5 (I-$A^{b,d,q}$; I-$E^{d,k}$) and AF6 (I-A^b)] and estimation of Ab K_D. (**B**) Assessment of VHH7 binding capacity to recombinant MHCII-CLIP variants by surface plasmon resonance. Multiple dilutions are shown for each MHCII–VHH7 interaction. K_a and K_d of VHH7 were calculated in combination with I-A^b, I-A^d, I-A^u, I-A^k, and I-A^{g7}. Binding to I-E locus was not detected (data not shown). Each figure is representative of two or three independent experiments. RU, resonance unit.

Author Manuscript Author Manuscript Author Manuscript Author Manuscript

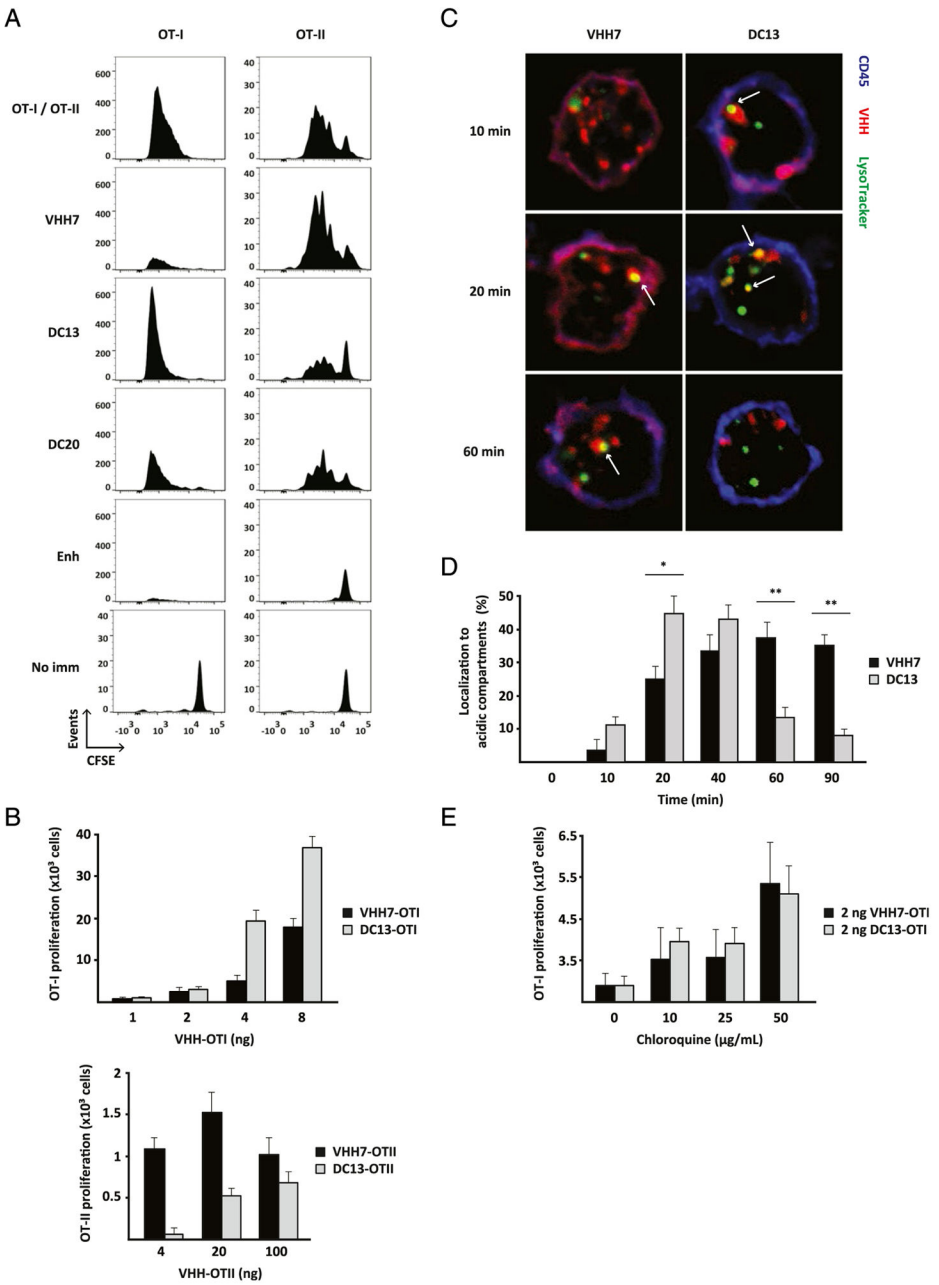

FIGURE 3.

Receptor-mediated T cell activation is independent of the DC subtype targeted. (**A**) CFSE-labeled OT-I CD8 T cells or OT-II CD4 T cells on a $Rag^{-/-}$ background were cocultured with splenic DCs in the presence of the respective OVA peptides: VHH7, DC13, DC20, or control VHH (Enh) fused to OT-I or OT-II epitopes. Cell proliferation was measured after 36 h by CFSE dilution and analyzed by FACS. OT-I T cells were gated on $TCR\beta^+$ $CD8^+$, and OT-II T cells were gated on $TCR\beta^+$ and $CD4^+$. Graphs show CFSE dilution in expanded OT-I/II T cells. (**B**) Quantification of OT-I or OT-II T cell proliferation after incubation of DCs previously stimulated with different concentrations of VHH7 and DC13 conjugates. (**C** and

Author Manuscript Author Manuscript Author Manuscript Author Manuscript

D) VHH7–MHCII and DC13–CD11b complexes are routed to acidic compartments and remain there for distinct time periods. (**C**) Confocal microscopy of internalization and intracellular distribution of VHH7 or DC13. DCs were incubated on ice with Alexa Fluor 647–labeled VHHs, washed, and incubated at 37°C for different time periods in the presence of LysoTracker. Before fixation, cells were costained with anti-CD45 mAb. Arrows denote colocalization of VHH and lysotracker. Original magnification ×~500. (**D**) Quantification of VHH constructs localized in acidic compartments after internalization. (**E**) Quantification of OT-I proliferation upon VHH7 or DC13-OTI stimulation of splenic DCs exposed to different concentrations of chloroquine. Each figure is representative of three independent experiments. $*p < 0.05$, $**p < 0.01$.

Author Manuscript Author Manuscript Author Manuscript Author Manuscript

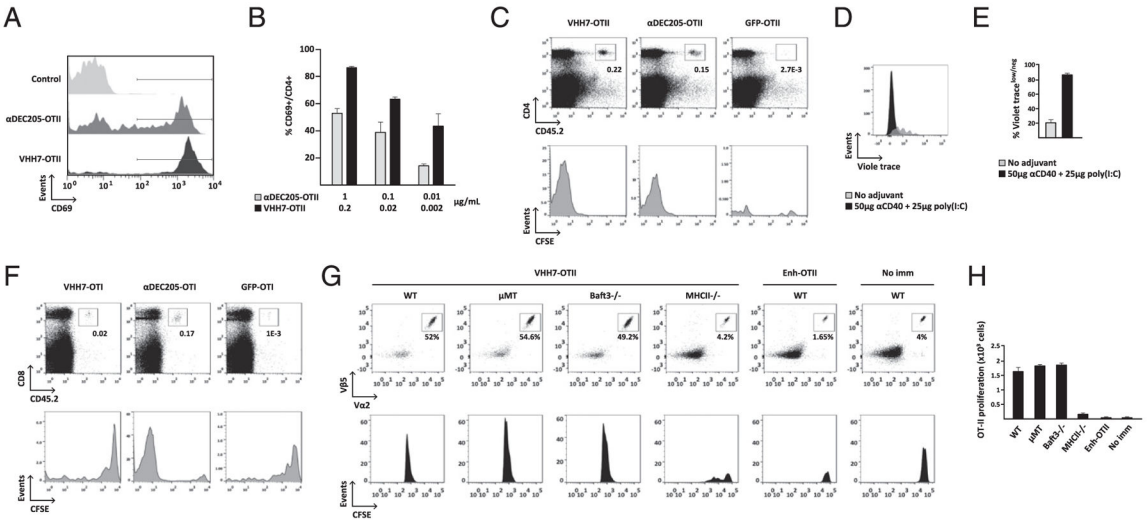

FIGURE 4.

Targeting of MHCII products via VHH7 fusions elicits strong CD4 T cell proliferation. (**A**–**C**) At equimolar concentrations, VHH7-OTII (0.2 μg) is more efficient at activating specific $CD4^+$ T cells than is anti-DEC205–OTII (1 μg), in vitro and in vivo. (**A** and **B**) DCs were incubated with OTII-specific CD4 T cells from OT-II–transgenic mice, and T cell activation was monitored by CD69 cell surface expression. (**A**) Graphs represent CD69 staining of OT-II T cells after incubation of DCs with equimolar concentrations of VHH7-OTII or anti-DEC205–OTII. (**B**) Quantification of CD69 surface expression in OT-II T cells after incubation of DCs with different concentrations of VHH7-OTII or anti-DEC205–OTII. (**C**) CFSE-labeled $CD4^+$ T cells from CD45.2 OT-II–transgenic mice were transferred i.v. into CD45.1 C57BL/6 mice ($n = 3$ per group). One day later, recipient mice were left untreated or were immunized with equimolar amounts of VHH7-OTII, anti-DEC205–OTII, or GFP-OTII in solution with 25 μg of anti-CD40 and 50 μg of poly(I:C). CD4 T cell expansion was measured by flow cytometry 7 d later. Staining of splenocytes with fluorescently labeled anti-CD4 and anti-CD45.2 shows stronger proliferation of anti-OTII CD4 T cells in VHH7-OTII–immunized mice. Graphs of donor OT-II CD45.2 cells show loss of CFSE labeling in proliferating cells. (**D** and **E**) In vivo targeting of VHH7-OTII with anti-CD40 and poly(I:C) induces stronger proliferation of OT-II CD4 T cells than does VHH7-OTII alone. (**D**) CellTrace Violet–labeled $CD4^+$ T cells from CD45.2 OT-II–transgenic mice were transferred i.v. into CD45.1 C57BL/6 mice ($n = 3$ per group). Immunization and readout are as in (**C**). (**E**) Quantification of CellTrace $Violet^{low/neg}$ OT-II T cells in (**D**). (**F**) VHH7-OTI fails to activate $CD8^+$ T cells in vivo. CFSE-labeled $CD8^+$ T cells from CD45.2 OT-I–transgenic mice were transferred i.v. into CD45.1 C57BL/6 mice ($n = 3$ per group). One day later, recipient mice were immunized with equimolar amounts of VHH7-OTI, anti-DEC205–OTI, or GFP-OTI in solution with 25 μg of anti-CD40 and 50 μg of poly(I:C) or were left untreated. OT-I expansion was assessed as in (**C**). (**G**) VHH7-OTII immunization activates $CD4^+$ T cells through $CD8^-$ DCs. CFSE-labeled OT-II $Rag^{-/-}$ CD4 T cells from OT-II–transgenic mice were transferred i.v. into C57BL/6 wild-type, μMT, $Baft3^{-/-}$, or $MHCII^{-/-}$ mice, followed by i.p. injection of VHH7-OTII in combination with anti-CD40 and poly(I:C). C57BL/6 wild-type mice immunized with Ehn-OTII or left untreated were used as

Author Manuscript Author Manuscript Author Manuscript Author Manuscript

controls. CD4 T cell expansion was measured by flow cytometry 3 d later. Graphs of donor OT-II cells were gated on Vβ5 and Vα2 TCR markers and show loss of CFSE labeling in expanded cells. (**H**) Quantification of OT-II T cell proliferation in (**G**). Graphs and dot-plots are representative of two or three independent experiments.

Author Manuscript Author Manuscript Author Manuscript Author Manuscript

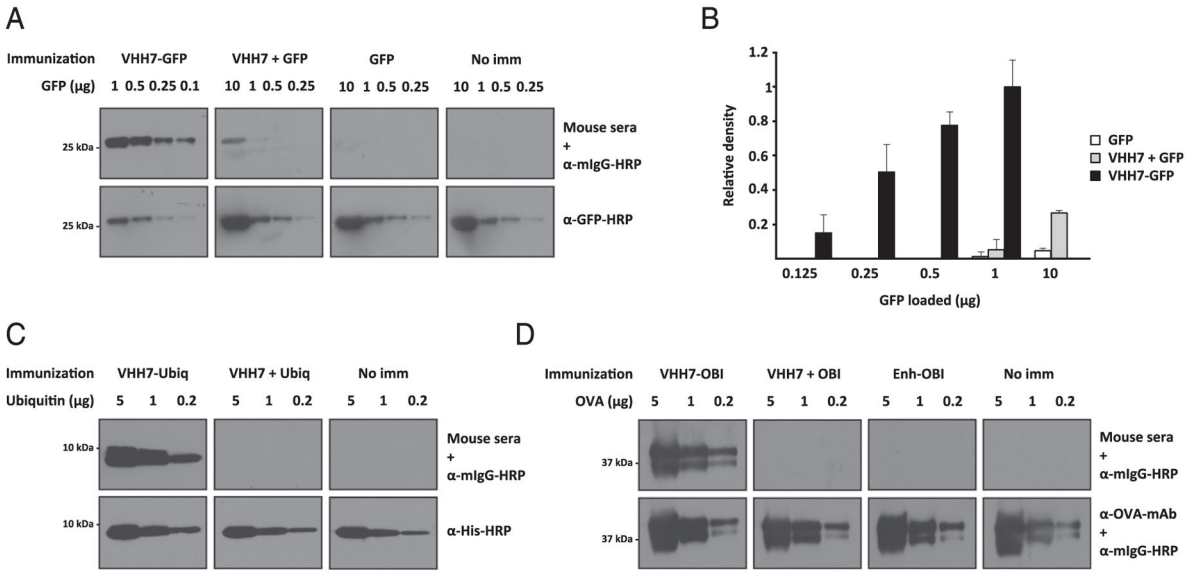

FIGURE 5.

In vivo Ag targeting via anti-MHCII VHH primes strong Ab responses against peptide epitopes. (**A** and **B**) VHH7 fused to GFP enhances serum response ~100-fold. (**A**) BALB/c mice were left untreated or were immunized with equimolar amounts of VHH7-GFP, unconjugated GFP, or GFP in solution with VHH7 (n = 3 per group). All mice were immunized i.p. at weeks 1, 3, and 5 with 25 μg of anti-CD40 and 50 μg of poly(I:C) as adjuvant, and blood was collected at week 6. Sera were immunoblotted against GFP at the indicated concentrations for VHH7-GFP fusion and up to 10 μg for VHH7 + GFP or GFP alone. Anti-GFP–HRP was used as control. (**B**) Quantification of densitometric traces of GFP detected by immunoblot using the sera from immunized mice. (**C**) Ab response against yeast ubiquitin. BALB/c mice were left untreated or were immunized with equimolar amounts of VHH7-ubiquitin or VHH7 mixed with ubiquitin (n = 3 per group). Sera were used for immunoblotting against various concentrations of His_6-tagged ubiquitin. Anti-His–HRP Ab was used as loading control. (**D**) Ab response against OBI-17mer peptide. BALB/c mice were left untreated or were immunized with equimolar amounts of VHH7-OBI 17-mer, OBI 17-mer in solution with VHH7, or control VHH fused to OBI (n = 3 per group). Sera were used for immunoblotting against intact OVA. Mouse anti-OVA Ab and anti-mouse IgG-HRP were used as loading controls. Each figure is representative of two or three independent experiments.

Author Manuscript Author Manuscript Author Manuscript Author Manuscript

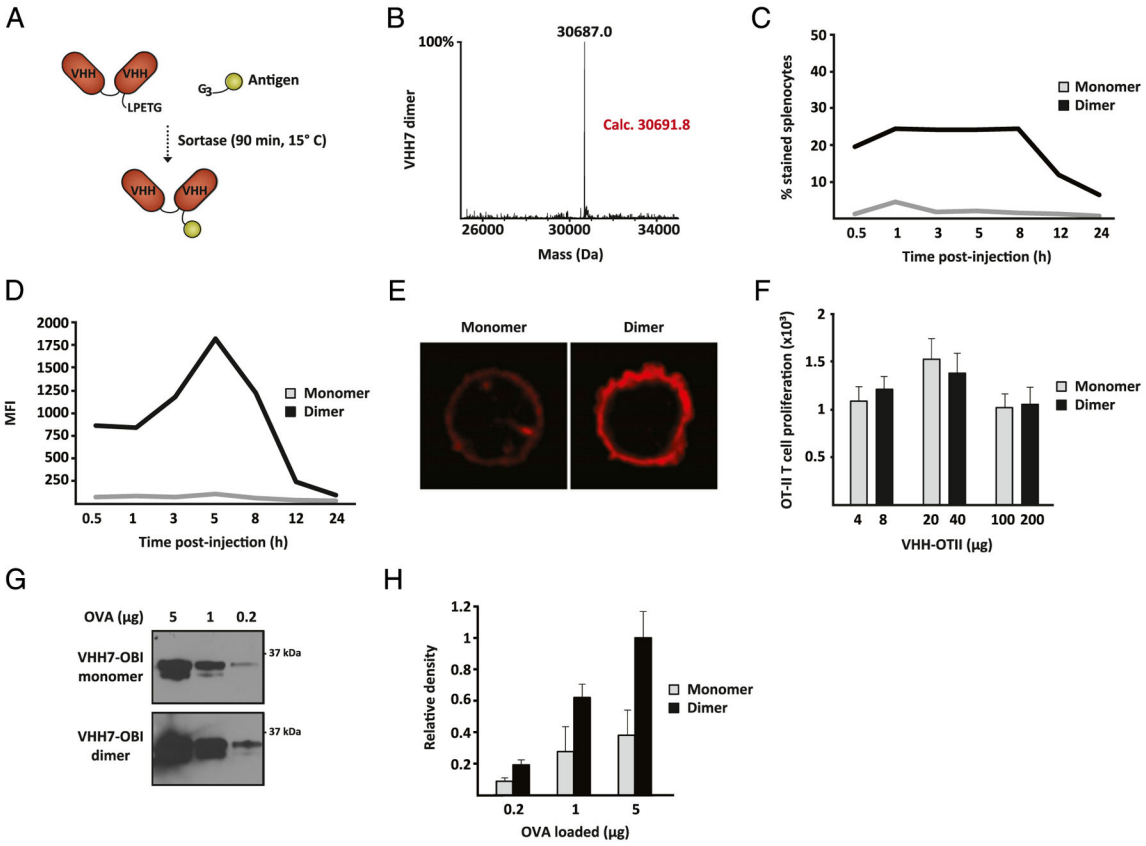

FIGURE 6.

Dimerization of VHH7 further enhances Ab response. (**A**) Schematic diagram of VHH7 dimer fusion to an Ag payload. (**B**) LC-MS of VHH7 dimer after Ni-NTA purification and SEC. (**C**–**E**) VHH7 homodimer shows superior avidity and half-life compared with monomeric VHH7. (**C**) Quanti-fication of splenocyte staining by cytofluorimetry of mice injected i.v. with monomeric or homodimeric versions of VHH7. (**D**) Mean fluorescence intensity of stained splenocytes in (**C**). (**E**) Comparative confocal microscopy of monomer- or dimer-stained splenocytes 1 h postinjection. (**F**) Quantification of OT-II T cell proliferation upon incubation of DCs with equimolar concentrations of OT-II coupled to VHH7 monomer or dimer. (**G** and **H**) VHH7 dimer enhances the Ab response against OBI-17mer peptide by ~2-fold compared with VHH7 monomer. (**G**) Immunization protocol as in Fig. 5D. (**H**) Quantification of densitometric traces of anti-OVA immunoblot using sera from immunized mice. Each figure is representative of two or three independent experiments.

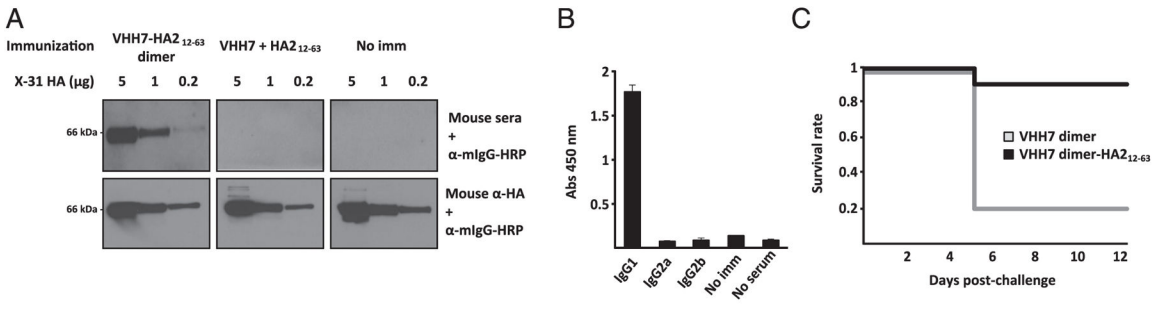

FIGURE 7.

In vivo protection against influenza infection. (**A** and **B**) Ab response against influenza's HA2 α-helix (H3N2 $HA2_{12–63}$). (**A**) BALB/c mice were left untreated or were immunized with equimolar amounts of VHH7 dimer–$HA2_{12–63}$ or peptide in solution with free VHH7 (n = 5 per group). Sera were used for immunoblotting against H3N2/X-31 recombinant HA. Mouse anti-HA and anti-mouse IgG Abs were used as control. (**B**) Sera from mice immunized with VHH7 dimer–$HA2_{12–63}$ produce IgG1, as measured by ELISA. Anti-IgG1–HRP was used in the control group (no immunization [no imm]). (**C**) Survival of mice after respiratory challenge with influenza A H3N2/X-31. BALB/c mice previously immunized with VHH7 dimer or VHH7 dimer–$HA2_{12–63}$ as in (**A**) were given 1.25×10^5 EID_{50} of H3N2/X-31 virus and monitored for 12 d postinoculation (n = 10 per group). Each figure is representative of two to four independent experiments.

Author Manuscript Author Manuscript Author Manuscript Author Manuscript